

# NEUTRINO EMISSION FROM COOPER PAIRS AND MINIMAL COOLING OF NEUTRON STARS

DANY PAGE

Departamento de Astrofísica Teórica, Instituto de Astronomía, Universidad Nacional Autónoma de México, 04510 Mexico D.F., Mexico

JAMES M. LATTIMER

Department of Physics and Astronomy, State University of New York at Stony Brook, Stony Brook, NY-11794-3800, USA

MADAPPA PRAKASH

Department of Physics and Astronomy, Ohio University, Athens, OH 45701-2979, USA

ANDREW W. STEINER

Joint Institute for Nuclear Astrophysics, National Superconducting Cyclotron Laboratory and,  
Department of Physics and Astronomy, Michigan State University, East Lansing, MI 48824, USA  
*Draft version October 22, 2018*

## ABSTRACT

The minimal cooling paradigm for neutron star cooling assumes that enhanced cooling due to neutrino emission from any direct Urca process, due either to nucleons or to exotica such as hyperons, Bose condensates, or deconfined quarks, does not occur. This scenario was developed to replace and extend the so-called standard cooling scenario to include neutrino emission from the Cooper pair breaking and formation processes that occur near the critical temperature for superfluid/superconductor pairing. Superfluidity is generally expected to exist in the neutron star interior, and Cooper-pair neutrino emission processes, which operate through both vector and axial channels, can dominate cooling in the minimal model. Neutron stars that have observed temperatures that are too low for their age than in the minimal cooling model for any combination of its parameters will imply that enhanced cooling is occurring. Previous studies showed that the observed temperatures of young, cooling, isolated neutron stars with ages between  $10^2$  and  $10^5$  years, with the possible exception of the pulsar in the supernova remnant CTA 1, are consistent with predictions of the minimal cooling paradigm as long as the neutron  $^3\text{P}_2$  pairing gap present in the stellar core is of moderate size.

Recently, it has been found that Cooper-pair neutrino emission from the vector channel is suppressed by a large factor, of order  $10^{-3}$ , compared to the original estimates that violated vector current conservation. We show that Cooper-pair neutrino emission remains, nevertheless, an efficient cooling mechanism through the axial channel. As a result, the elimination of neutrino emission from Cooper-paired nucleons through the vector channel has only minor effects on the long-term cooling of neutron stars within the minimal cooling paradigm. We further quantify precisely the effect of the size of the neutron  $^3\text{P}_2$  gap and demonstrate that consistency between observations and the minimal cooling paradigm requires that the critical temperature  $T_c$  for this gap covers a range of values between  $T_c^{\min} \lesssim 0.2 \times 10^9$  K up to  $T_c^{\max} \gtrsim 0.5 \times 10^9$  K in the core of the star. This range of values guarantees that the Cooper-pair neutrino emission is operating efficiently in stars with ages between  $10^3$  to  $10^5$  years, leading to the coldest predicted temperatures for young neutron stars. In addition, it is required that young neutron stars have heterogeneous envelope compositions: some must have light-element compositions and others must have heavy-element compositions. Unless these two conditions are fulfilled, about half of the observed young cooling neutron stars are inconsistent with the minimal cooling paradigm and provide evidence for the existence of enhanced cooling.

*Subject headings:* Dense matter — equation of state — neutrinos — stars: neutron

## 1. INTRODUCTION

Neutron stars older than several minutes cool through a combination of emission of neutrinos from their interiors and photons from their surfaces. The former dominates the energy losses during the first  $\sim 10^5$  years after birth, but the latter is responsible for the observed thermal emissions detected from several neutron stars older than hundreds of years. For neutron stars of this age and older, the effective surface temperatures are tightly coupled to the interior temperatures, and the observability of these stars therefore depends crucially on the overall rate of neutrino emissions

Electronic address: page@astro.unam.mx  
Electronic address: lattimer@astro.sunysb.edu  
Electronic address: prakash@harsha.phy.ohiou.edu  
Electronic address: steinera@pa.msu.edu

from within the star.

Historically, theoretical neutron star cooling models have fallen into two categories, “standard” cooling or enhanced cooling (see, e.g. Pethick 1992, Prakash 1994, 1998, Page et al. 2006, and Page 2009). Standard cooling implies that no enhanced neutrino emissions from any direct Urca processes (Lattimer et al. 1991 and Prakash et al. 1992), due either to nucleons or to exotica such as hyperons, Bose condensates or deconfined quarks, occurs. Page et al. (2004) (hereafter referred to as Paper I) introduced the minimal cooling paradigm to address the question of whether or not there exists observational evidence that firmly indicates that enhanced cooling takes place in some neutron stars.

Traditionally, the standard cooling scenario has included only the modified Urca process (Friman & Maxwell 1979; Tsuruta 1986). However, over the last decade it has been realized that another important cooling mechanism is provided by Cooper pair breaking and formation (Flowers, Ruderman & Sutherland 1976; Voskresensky & Senatorov 1987), termed as the “PBF” process, which occurs in the presence of superconductivity or superfluidity in dense matter. It is generally accepted that superfluidity occurs in neutron star matter, although the magnitudes of the superfluid gap energies as a function of density are still uncertain at present. Furthermore, for temperatures near the associated superfluid critical temperatures, emission from Cooper pairs dominates the neutrino emissivities in many cases. Therefore, in the minimal cooling paradigm, neutrino emission is included both from modified Urca and bremsstrahlung processes as well as from the Cooper pair breaking and formation processes. Enhanced cooling is assumed not to occur. Any neutron star that has an observed surface temperature too low for its age than that predicted by the minimal cooling model for any combination of its input ingredients therefore implies that enhanced cooling as defined above has occurred in that star.

Using the rates for Cooper-pair processes established by previous authors (Yakovlev, Kaminker & Levenfish 1999; Kaminker, Haensel & Yakovlev 1999), Paper I concluded that with the possible exception of the pulsar in 3C58<sup>1</sup> and CTA 1, all cooling neutron stars for which thermal emissions have been detected are marginally consistent with the assumption that enhanced cooling is absent, given the combined uncertainties in ages and temperatures or luminosities. Importantly, it was concluded that overall consistency with minimal cooling was possible only if the neutron  $^3P_2$  gap was similar to our model “a” in Paper I, i.e., with critical temperatures of the order of  $10^9$  K.

This result was not sensitive to the neutron star mass or to the sizes of the n and p  $^1S_0$  gaps. In the case that the n  $^3P_2$  gap was significantly larger than this value, theoretical models yielded too slow cooling to account for the low temperatures of about half of the young neutron stars so far observed in thermal emission. It is also apparent from the results of Paper I that overall consistency with minimal cooling requires heterogeneity in envelope compositions for the young stars: light element compositions for some and heavy element compositions for others. One of the purposes of this paper is to show that, besides not being too large, the n  $^3P_2$  gap should also be not too small. Unless the n  $^3P_2$  lies in a narrow range, and there is heterogeneity in young neutron star envelopes, the implication is that about half of the observed young neutron stars with thermal emission have some degree of enhanced cooling.

Of course, even if the conditions on the neutron  $^3P_2$  gap and envelope compositions are met, the overall consistency of the minimal cooling paradigm with observations does not necessarily mean that direct Urca processes are forbidden. Direct Urca processes may in fact still occur in many stars, but those neutron stars would quickly grow too cold to be detectable from their thermal emissions (Page & Applegate 1992).

Pairing is expected to appear at low Fermi momenta ( $k_F \lesssim 1.5 \text{ fm}^{-1}$ ) in the singlet  $^1S_0$  state (Bohr, Mottelson & Pines 1958) and in the triplet  $^3P_2$ - $^3F_2$  mixed channel at higher momenta (Takatsuka 1972). In both cases, singlet or triplet, Cooper-pair emission can occur through the vector or the axial channel. The conservation of vector current in dense superfluid neutron matter was first addressed by Kunku & Reddy (2004). Recently, Leinson & Perez (2006a) have demonstrated that the vector part of the Cooper-pair emission in a one-component system of paired fermions is suppressed by a factor of  $\sim (1/20)(v_F/c)^4 \sim 10^{-3}$  relative to the original estimates of Flowers, Ruderman & Sutherland (1976), where  $v_F$  is the velocity of particles at the Fermi surface and  $c$  the speed of light. Leinson & Perez (2006a) have identified the key reason for this large suppression in one-component matter: in their original work, Flowers, Ruderman & Sutherland (1976) employed the bare vertex in the vector weak current; however, the use of the bare vertex violates vector current conservation. The conservation of vector current is achieved by including collective effects which minimally requires (in order to satisfy the Ward identity) that the correction to the bare vertex is calculated to the same order of approximation as the quasi-particle propagator is modified by the pairing interaction in the system.

The large suppression in the vector channel has been confirmed by additional works (Sedrakian, Müther & Schuck 2007; Kolomeitsev & Voskresensky 2008; Leinson 2008; Steiner & Reddy 2008). If the total Cooper-pair emission were suppressed by this factor, significant changes to results of the minimal cooling model might be anticipated. However, Cooper-pair emission occurs through both vector and axial channels, and the axial part of the Cooper-pair emission, which is proportional to  $v_F^3$ , is only slightly modified. Also, the rate of Cooper pair emission from the triplet configuration, being due to axial currents, is largely unaffected by these new results. A cursory examination of the results of Paper I suggests additional reasons that the revised Cooper-pair rates might not have a major influence on the minimal cooling scenario. One reason is that the specific heat of matter with superfluidity is not affected by the existence or absence of Cooper-pair emission. As a result, the cooling associated with  $^1S_0$  neutrons, which is confined to the crust, has only a transitory effect that is important during the crust’s thermal relaxation (i.e., during the first few hundred years at most). Another reason is that the cooling associated with the  $^1S_0$  protons in the stellar

<sup>1</sup> In view of the recent revisions in its age, the luminosity of this object now lies close to the cooling curves of the minimal paradigm.

core proceeds predominantly through the axial channel. Nevertheless, the large magnitude of the vector suppression suggests that a quantitative re-analysis of the cooling is in order to confirm these expectations.

The purposes of this paper are to (i) assess the effects of the suppression of Cooper pair neutrino emission in the vector channel on neutron star cooling and to examine their effects on the minimal cooling paradigm, (ii) critically evaluate the extent to which current data are compatible with the minimal cooling paradigm, (iii) highlight the crucial role of triplet pairing (found in Paper I) in more quantitative terms, and (iv) emphasize that young neutron stars cannot have identical envelope compositions and remain compatible with the minimal cooling paradigm.

In presenting our results below, the key ingredients of the minimal model in Paper I are retained. In doing so, we utilize the same (i) equation of state, (ii) superfluid properties of the relevant components, (iii) envelope composition, and (iv) stellar mass as in Paper I. We note that in a neutron star crust, which is a multi-component system, the neutron PBF emissivity might be modified by the lattice (Steiner & Reddy 2008). However, this effect has not yet been computed in detail. For the purposes of this work, we will assume that the modification in the speed of sound is small, and, thus, the  $v_F^4$  suppression in the vector channel for homogeneous bulk matter holds in general. The neutrino emissivities from the PBF processes will be altered to those calculated recently so that an apposite comparison with Paper I can be made. Where appropriate, new inputs with regard to superfluid gaps and revisions in data from observations will be utilized and so indicated.

## 2. PBF NEUTRINO EMISSIVITIES

As the temperature nears the critical temperature  $T_c$  for pairing, new channels for neutrino emission through the continuous formation and breaking of Cooper pairs (Flowers, Ruderman & Sutherland 1976; Voskresensky & Senatorov 1987) become operative.

The PBF emissivity for both neutrons ( $i = n$ ) and protons ( $i = p$ ) in the singlet ( $j = s$ ) and triplet ( $j = t$ ) channels (we only consider  $m_J = 0$ ) can be written in the form (Flowers, Ruderman & Sutherland 1976; Yakovlev, Kaminker & Levenfish 1999)

$$Q = \frac{4G_F^2 m_i^* p_{F,i}}{15\pi^5 \hbar^{10} c^6} (k_B T)^7 \mathcal{N}_\nu a_{i,j} F_j [\Delta_i(T)/T], \quad (1)$$

where  $G_F$  is the Fermi weak-interaction constant,  $m_i^*$  are effective masses,  $p_{F,i}$  are Fermi momenta,  $T$  is the temperature,  $\mathcal{N}_\nu$  is the number of neutrino flavors,  $a_{i,j}$  are factors involving vector and axial coupling constants and  $F_j$  are functions that depend on the temperature dependent pairing gaps  $\Delta_i(T)$  and control the efficiency of the PBF process. The functional forms of the gaps  $\Delta_i(T)$  are discussed in §3.3 of Paper I. Taking  $\mathcal{N}_\nu = 3$

$$Q = 3.51 \times 10^{21} \frac{\text{erg}}{\text{cm}^3 \text{ s}} \left( \frac{m_i^*}{m_i} \right) \left( \frac{p_{F,i}}{m_i c} \right) \times T_9^7 a_{i,j} F_j [\Delta_i(T)/T], \quad (2)$$

where  $m_i$  are the bare masses, and the control functions  $F_s$  and  $F_t$  (for  $m_J = 0$ ) are (Yakovlev, Kaminker & Levenfish 1999)

$$F_s = y^2 \int_0^\infty \frac{z^4 dx}{(1 + ez)^2} \quad (3)$$

$$F_t = \frac{1}{4\pi} \int d\Omega y^2 \int_0^\infty \frac{z^4 dx}{(1 + ez)^2} \quad (4)$$

where  $y = \Delta_i(T)/T$ ,  $z = \sqrt{x^2 + y^2}$ , and  $\int d\Omega$  represents the angle averaging procedure detailed in Yakovlev, Kaminker & Levenfish (1999). The form of the control functions  $F_s$  and  $F_t$  shown in Figure 13 of Paper I clearly shows that the PBF process turns on when  $T$  reaches  $T_c$ , increases its efficiency as  $T$  decreases, and becomes exponentially suppressed when the gap approaches its maximum size  $\Delta(T = 0)$  when  $T \lesssim 0.2T_c$ .

As we wish to examine the extent to which the cooling curves are altered by PBF emissivities that incorporate the conservation of the weak vector current, we collect below the relevant results for the factors  $a_{i,j}$ .

*Vector current not conserved:* For the singlet and triplet configurations, the factors  $a_{i,j}$  (including both vector and axial parts) have the values (Yakovlev, Kaminker & Levenfish 1999; Kaminker, Haensel & Yakovlev 1999)

$$a_{n,s} = C_{V,n}^2 + C_{A,n}^2 \tilde{p}_{F,n}^2 \left( 1 + \frac{11}{42} \tilde{m}_n^{-2} \right) \quad (5)$$

$$a_{p,s} = C_{V,p}^2 + C_{A,p}^2 \tilde{p}_{F,n}^2 \left( 1 + \frac{11}{42} \tilde{m}_p^{-2} \right) \quad (6)$$

$$a_{n,t} = C_{V,n}^2 + 2C_{A,n}^2 \quad (7)$$

$$a_{p,t} = C_{V,p}^2 + 2C_{A,p}^2, \quad (8)$$

where  $\tilde{p}_{F,i} \equiv p_{F,i}/m_i$  and  $\tilde{m}_i \equiv m_i^*/m_i$ .

*Vector current conserved:* Enforcing the Ward identity suppresses the vector parts of the PBF emissivities (Leinson & Perez 2006a). The suppression in the vector part of the singlet channel is proportional to

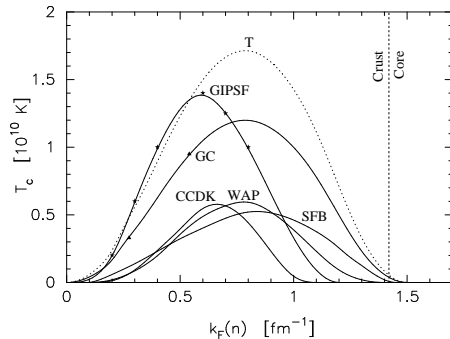


FIG. 1.— Representative neutron  $^1S_0$  pairing critical temperature  $T_c$  as a function of the neutron Fermi momentum  $k_F$  from various calculations: Takatsuka (1972) (“T”), a calculation within the BCS approximation; Wambach, Ainsworth & Pines (1993) (“WAP”), Chen, et al. (1993) (“CCDK”), and Schwenk, Friman & Brown (2003) (“SFB”), which take into account medium polarization beyond the BCS level; Gezerlis & Carlson (2008) (“GC”) and Gandolfi, et al. (2008) (“GIPSF”) denote Quantum Monte-Carlo results (as these latter results, marked as triangles and stars, respectively, are restricted to relatively low densities, we have extrapolated them to higher densities). In all cases,  $T_c$  was obtained from the zero temperature gap  $\Delta(0)$  through the standard BCS result as  $k_B T_c = 0.57\Delta(0)$ . The vertical dotted line shows the location of the crust-core boundary.

$(4/81)v_{F,i}^4$  (Kolomeitsev & Voskresensky 2008), where  $v_{F,i} = p_{F,i}/m_i^*$  are the Fermi velocities. The suppression of the vector part in the triplet channel is also strong, so we set the contribution from the vector part to zero as done in Leinson & Perez (2006b). Consequently, the quantities  $a_{i,j}$  are modified to

$$a_{n,s} = C_{V,n}^2 \left(\frac{4}{81}\right) \left(\frac{v_{F,n}}{c}\right)^4 + C_{A,n}^2 \tilde{p}_{F,n}^2 \left(1 + \frac{11}{42}\tilde{m}_n^{-2}\right) \quad (9)$$

$$a_{p,s} = C_{V,p}^2 \left(\frac{4}{81}\right) \left(\frac{v_{F,p}}{c}\right)^4 + C_{A,p}^2 \tilde{p}_{F,p}^2 \left(1 + \frac{11}{42}\tilde{m}_p^{-2}\right) \quad (10)$$

$$a_{n,t} = 2C_{A,n}^2 \quad \text{and} \quad a_{p,t} = 2C_{A,p}^2. \quad (11)$$

The values of the various coupling constants are  $C_{V,n} = 1$ ,  $C_{A,n} = g_A$ ,  $C_{V,p} = 4\sin^2\theta_W - 1$ , and  $C_{A,p} = -g_A$ , where  $g_A \approx 1.26$  and  $\sin^2\theta_W \approx 0.23$ . Notice that  $C_{V,p}^2 \ll C_{V,n}^2$ , whereas  $C_{A,p}^2 = C_{A,n}^2$ . The fact that  $\tilde{p}_{F,p} \ll \tilde{p}_{F,n}$ , implies that neutrino emission from the PBF process involving triplet neutron pairing is intrinsically much more efficient than that from singlet proton pairing.

Although the neutron pairing at high densities involves a mixing of the  $^3P_2$  and  $^3F_2$  channels (Takatsuka 1972), this mixing is not taken into account in the triplet PBF emissivities quoted above. In what follows, we will simply refer to the pairing of neutrons at high densities as  $^3P_2$  pairing.

### 3. EFFECTS OF PAIRING AND PBF EMISSIVITIES

The most significant revision of PBF neutrino emission is in the case of the neutron  $^1S_0$  pairing as emission from the  $^3P_2$  pairing is suppressed only by about 30%. Comparison of equations (5) through (8) with equations (9) through (12) shows that the total emissivity from the proton  $^1S_0$  pairing is essentially unaffected as it is largely dominated by the axial channel. Both proton  $^1S_0$  and neutron  $^3P_2$  pairings occur in the core, which contains more than 90% of the star’s volume, whereas the neutron  $^1S_0$  pairing is essentially restricted to the crust. We now assess how the predicted large suppression in the vector channel for the various gaps affects the minimal cooling paradigm.

#### 3.1. Effect of the neutron $^1S_0$ gap in the crust

There are substantial variations in model predictions for the  $^1S_0$  gap. For the models we use, Figure 1 summarizes predictions for the superfluid critical temperatures  $T_c$  as a function of the neutron Fermi momentum  $k_F(n)$ , including results of two new calculations performed after Paper I was written. The neutron  $^1S_0$  gap is mostly confined to the stellar crust, which constitutes only a small fraction of the stellar volume. As a result, effects of the suppression are mostly observed during the thermal relaxation of the crust (Lattimer et al. 1994; Page 2009). We therefore focus on the first  $10^3$  years of evolution during which the effects of suppression are most evident (see Figure 2).

We begin with a stellar model in which no pairing is taken into account (curve 1 in Figure 2). In this case, the crust’s early cooling is driven by neutrino emission from the plasmon process and the neutron-neutron bremsstrahlung from the (unpaired) neutrons in the inner crust, with a small contribution from the electron-ion (and a smaller one from electron-electron) bremsstrahlung process.

In the presence of a neutron  $^1S_0$  gap, three effects appear: suppression of the (inner crust) neutron specific heat, suppression of the  $n-n$  bremsstrahlung, and the onset of the PBF process. We illustrate the influence of these three effects in succession in Figure 2. Curve 2 includes only the suppression of the specific heat, which results in a direct shortening of the thermal relaxation time of the crust. Curve 3 adds the  $n-n$  bremsstrahlung suppression, which results in a higher temperature and hence a lengthening of the relaxation phase. Curves 4 and 5 show the total effect

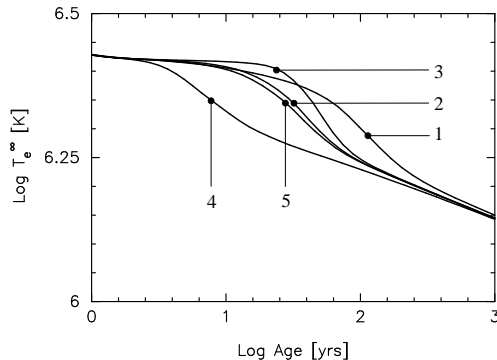


FIG. 2.— Comparison of cooling during the crust thermal relaxation era including various effects from neutron  $^1S_0$  pairing. The  $^1S_0$  gap “SFB” from Schwenk, Friman & Brown (2003) has been employed. No pairing in the core has been included and the star is a  $1.4 M_\odot$  star built with the EOS of APR (Akmal, Pandharipande & Ravenhall 1998) and has a heavy element envelope (see Paper I). Curves 1 through 5 are explained in the text.

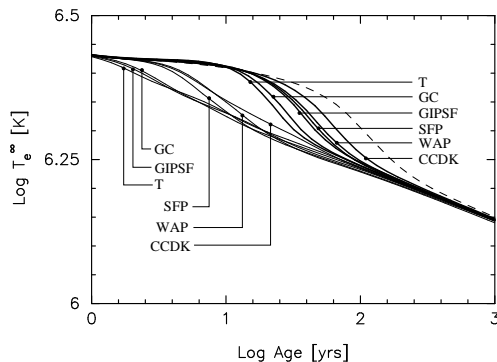


FIG. 3.— Early cooling of a neutron star with various neutron  $^1S_0$  gaps. Upper (thick) curves take into account the suppression of the vector channel of the PBF process (as in curve 5 of Figure 2) whereas, for comparison, the lower (thin) curves are without the suppression (as in curve 4 of Figure 2). The dashed curve show the cooling in absence of neutron pairing (as in curve 1 in Figure 2). Notation for gaps is the same as in Figure 1.

of the neutron  $^1S_0$  pairing by also taking into account the PBF emission process. For comparison, curve 4 is the result in which the vector channel contribution is assumed to be unsuppressed whereas curve 5 takes this suppression into account. As had been anticipated, the suppression of the vector channel of the PBF process has a significant effect, but only at early times ( $t < 1000$  years), and results in warmer crusts and increased crust relaxation times. However, after crust relaxation is attained, the differences among cooling histories of the various models is very small (this is more clearly illustrated below in Figure 8).

In order to demonstrate that this result is independent of the specific character of the  $^1S_0$  gap, we compare in Figure 3 the cooling during the crust thermal relaxation era using the various models for this gap from Figure 1. Although quantitative differences are apparent, the qualitative nature of the effects of suppression are the same for all gaps.

The effects of vector suppression are therefore likely to be important in the interpretation of neutron star crustal cooling observed in X-ray transients from accretion-heated neutron stars in Low-Mass X-ray Binaries (Cackett, et al. 2006, 2008; Degenaar, et al. 2009) as the crustal cooling timescale is sensitive to the neutrino emission rates (Lattimer et al. 1994; Rutledge, et al. 2002; Shternin, et al. 2007; Brown, & Cumming 2009). Inasmuch as the inclusion of the effects of vector suppression increases the cooling timescale, the inferred crust thickness will be overestimated if these effects are ignored. Likewise, higher temperatures can be reached in the crust of an accreting neutron star once the vector suppression of the PBF rate is taken into account and has important consequence for the triggering of superbursts (Cumming, et al. 2006).

We therefore conclude that the suppression of the vector channel of the neutron  $^1S_0$  PBF process does not lead to a distinguishable effect in the long-term cooling ( $> 1000$  years) of the star.

### 3.2. Effects of the neutron $^3P_2$ and proton $^1S_0$ gaps in the core

We now compare the relative efficiencies of the PBF processes from the neutron  $^3P_2$  and/or proton  $^1S_0$  Cooper pairs with the modified Urca processes (neutron and proton branches) and nucleon bremsstrahlung processes in the core. In Figure 4, we plot the two families of gaps we will consider. As discussed in Paper I, these gaps cover the broad range of predicted values from microscopic calculations. Particularly uncertain is the maximum size of the neutron  $^3P_2$  gap, as well as the range in density over which it is significant (Schwenk & Friman 2004; Baldo et al. 1998).

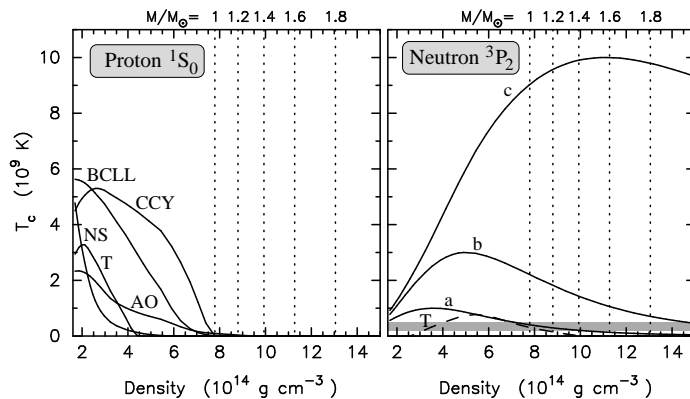


FIG. 4.— Critical temperature,  $T_c$ , for the proton  $^1S_0$  gaps, left panel, and neutron  $^3P_2$  gaps, used in this work. These are the same gaps as shown in Figure 9 and 10 of Paper I, respectively, but displayed as functions of the matter density  $\rho$  instead of particle Fermi momenta,  $k_F$ , as in Paper I. Conversion from  $k_F$  to  $\rho$  was performed with the APR EOS and its corresponding proton fraction. This conversion is only weakly dependent on the EOS given the constraints imposed by the conditions of minimal cooling on the EOS. Central densities of stars with masses from 1 to  $1.8 M_\odot$  are indicated. The grey strip for the neutron  $^3P_2$  gaps is the *compatibility band* discussed in §3.3. See Paper I for references.

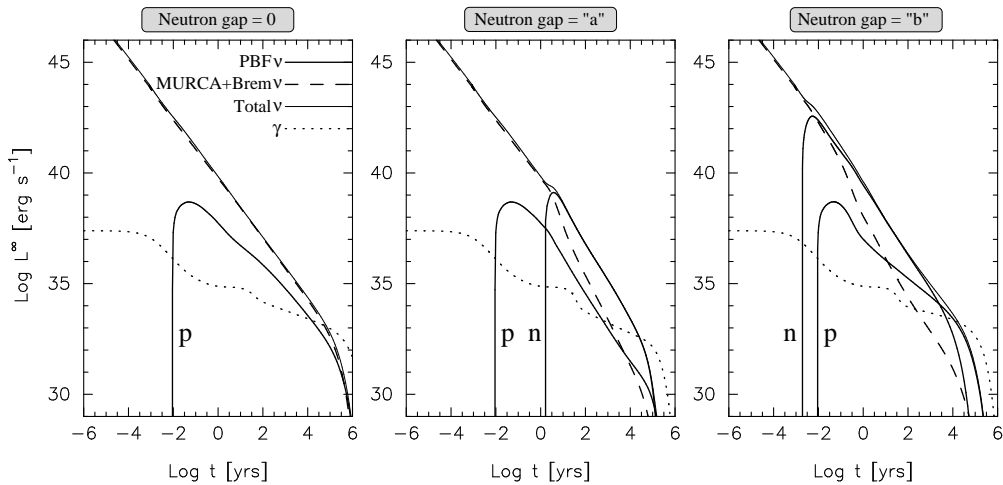


FIG. 5.— Comparison of luminosities from various processes during three realistic cooling histories: photon (“ $\gamma$ ”), all  $\nu$ -processes (“Total  $\nu$ ”), modified Urca and nucleon bremsstrahlung (“MURCA+Brem  $\nu$ ”), and PBF (“PBF  $\nu$ ”) from neutron  $^3P_2$  (“n”) and proton  $^1S_0$  (“p”) pairing. PBF neutrino emission from the neutron  $^1S_0$  gap is not shown explicitly as its contribution is always dominated by other processes, but is included in the total  $\nu$  luminosity. Suppression of the vector channel of the PBF processes is properly taken into account in all cases. In all cases shown, the proton  $^1S_0$  gap is from Amundsen & Østgaard (1985a) (model “AO” in Figure 4) and the neutron  $^1S_0$  gap from Schwenk, Friman & Brown (2003) (model “SFB” in Figure 1). The neutron  $^3P_2$  gap is chosen to be vanishingly small (left panel), from our model “a” (center), or model “b” (right) from Figure 4. The star is a  $1.4 M_\odot$  star built with the EOS of APR (Akmal, Pandharipande & Ravenhall 1998) and has a heavy element envelope (see Paper I).

As an example, we choose the proton  $^1S_0$  gap from model “AO” of Figure 4 and we consider three neutron  $^3P_2$  gaps: one vanishingly small, and the two models “a” and “b” from the same figure, which have maximum values of  $T_c = 10^9$  K and  $3 \times 10^9$  K, respectively. Figure 5 shows the resulting neutrino and photon luminosities in full cooling calculations. In the case of a vanishing neutron  $^3P_2$  gap (left panel), the only PBF process occurring in the core is from the proton  $^1S_0$  pairing, but due to its intrinsically low efficiency it cannot compete with the modified Urca process which is unsuppressed in the inner core where the proton gap vanishes. This model is very similar to the old “standard cooling” case. The other two panels in Figure 5 with non-vanishing neutron  $^3P_2$  gaps clearly show that the PBF processes dominate the total neutrino luminosity as soon as the neutron  $^3P_2$  pairing appears.

It is worthwhile to note the competition between the proton  $^1S_0$  and neutron  $^3P_2$  PBF processes which depends on the relative sizes of the gaps. For a large neutron  $^3P_2$  gap, as our case “b” used to obtain the luminosities in the right panel of Figure 5, the temperature of the entire core drops below  $T_c$  in a short time; thereafter, the corresponding PBF process is suppressed. When neutrons in the entire core are well into the superfluid phase the PBF process from the proton  $^1S_0$  gap subsequently drives the cooling, at ages  $\gtrsim 10^3$  yrs, but with a low efficiency. In contrast, when the neutron  $^3P_2$  model gap “a” is used to obtain the luminosities in the central panel of Figure 5, neutrino emission from the neutron PBF process largely dominates the cooling. As noted in Paper I, such gaps as “a” lead to the coldest minimal cooling neutron stars.

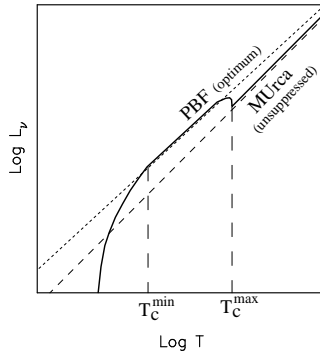


FIG. 6.— A schematic diagram of the neutrino luminosity as a function of temperature for the modified Urca and PBF processes. The dotted curve shows the optimal PBF luminosity (i.e., obtainable when a thick enough layer in the core has its temperature close to  $T_c$ ) and the dashed curve shows the unsuppressed MUrca luminosity. The values of  $T_c^{\min}$  and  $T_c^{\max}$  are the minimum and maximum values of  $T_c$  for the neutron  ${}^3P_2$  gap (which is a function of density) that occur within the star. When the temperature in the core falls below  $T_c^{\max}$  the neutrino luminosity at that point increases to the PBF luminosity, which can be almost two orders of magnitude higher than the MUrca luminosity in the optimal case. When the temperature falls further, to below  $T_c^{\min}$ , the neutrino luminosities from both the PBF and MUrca process are quenched. (Figure inspired from Figure 20 of Paper I.)

### 3.3. Characterization of the most efficient neutron ${}^3P_2$ gaps in the core

The most efficient pairing configurations, which lead to the coldest neutron stars, a situation explored in Paper I, are neutron  ${}^3P_2$  gaps with  $T_c$  values around  $10^9$  K in the largest possible fraction of the core (as in the case of our model “a”). In this case, the efficient PBF process from the neutron  ${}^3P_2$  gap dominates the neutrino luminosity at ages  $\sim 10^0 - 10^5$  yrs (as seen in the central panel of Figure 5) and results in the coldest young neutron stars within the minimal cooling paradigm.

The schematic illustration in Figure 6 shows the neutrino luminosity as a function of temperature for the modified Urca and PBF processes. As long as the temperature is greater than  $T_c^{\max}$ , which we define as the maximum value of  $T_c$  in the core, the modified Urca process drives the cooling. When the temperature falls below  $T_c^{\max}$ , the PBF process turns on and dominates the cooling, until the temperature drops below  $T_c^{\min}$ , which we define as the minimum value of  $T_c$  in the core, when both the PBF and modified Urca processes are quenched everywhere in the core.

The surface temperature at early times is controlled by crustal physics, as described in §3.1, and is independent of the evolution of the core. For the surface temperature to reach the smallest possible values, the value of  $T_c^{\max}$  should be large enough for the PBF process to turn on before, or not much later than, the crust isothermization time. A useful reference age is  $\sim 10^3$  years, the estimated age of the youngest observed cooling neutron stars, for the PBF process to be fully operating. At later times, if the value of  $T_c^{\min}$  is too large both the PBF and modified Urca processes will turn off before the photon cooling era and the cooling will proceed at a slower pace. This feature is illustrated in Figure 7 which shows cooling curves for various neutron  ${}^3P_2$  gaps. The upper solid curve shows cooling for the case in which the neutron  ${}^3P_2$  gap is zero ( $\Delta = 0$ ). The lower solid curve shows cooling for a neutron  ${}^3P_2$  gap corresponding to case “a”, which is close to the most efficient case, giving the lowest temperatures at all ages. The corresponding values of  $T_c^{\max}$  and  $T_c^{\min}$  in the  $1.4 M_\odot$  star used in Figure 7 are  $10^9$  K and  $2 \times 10^8$  K, respectively. The three models “0.6a”, “0.4a”, and “0.2a”, in Figure 7 with scaled down gaps show that to obtain the coldest star  $T_c^{\max}$  should be at least about 0.5 times the  $T_c^{\max}$  value of model “a”, that is,

$$T_c^{\max} > 0.5 \times 10^9 \text{ K.} \quad (12)$$

With respect to the optimal value of  $T_c^{\min}$ , the model “2.0a” in Figure 7 with a scaled up gap shows that the turning off of both modified Urca and PBF processes occurs somewhat too early, resulting in warmer stars at ages  $> 10^3$  years. Consequently,  $T_c^{\min}$  should not be much larger than that of our model “a” for this particular  $1.4 M_\odot$  star:

$$T_c^{\min} \lesssim 0.2 \times 10^9 \text{ K.} \quad (13)$$

The two bounds in equations 12 and 13 allow us to draw a “compatibility band” for the  $T_c$  curve, shown as a horizontal grey strip in the right panel of Figure 4. A  $T_c$  curve will yield the coldest possible minimally cooling neutron star, at ages between  $10^3$  to a few times  $10^4$  years, only if it crosses the compatibility band within the density range present in the core of the star. Examination of Figure 4 shows that neutron  ${}^3P_2$  gaps resembling those of model “a” provide the most efficient cooling for neutron stars of masses close to 1.4 solar masses.

In order to assess the role of the gap’s density dependence, we also performed cooling simulations using the neutron  ${}^3P_2$  gap “T” (from Takatsuka 1972) of Figure 4. This gap model is similar to our model “a”, but the density dependence is different. It has  $T_c^{\max} = 0.75 \times 10^9$  K and  $T_c^{\min} = 0$ , this minimum being reached at low densities, and thus crosses the compatibility band. Cooling simulations utilizing models “a” and “T” result in virtually identical trajectories. In contradistinction to the lower bound of equation (12), it is not possible to have an upper bound on  $T_c^{\max}$ , the only condition being that the  $T_c$  curve must cross the compatibility band. Notice that a gap with a density dependence similar to our models “b” and “c” and a very large  $T_c^{\max} (\gg 0.5 \times 10^9 \text{ K})$  is also likely to have a very large  $T_c^{\min}$ , and

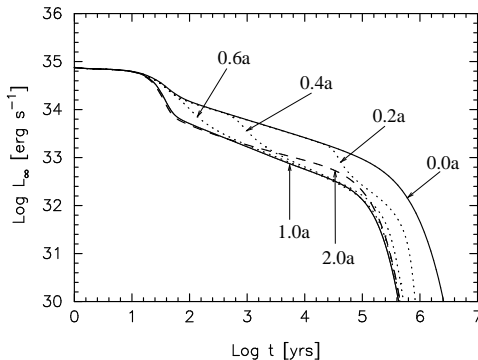


FIG. 7.— Comparison of predictions of the minimal cooling scenario for variations of the neutron  ${}^3\text{P}_2$  gap. We take as a reference gap our model “a” for Figure 4 which we scale by a factor “s”; curves are labelled by this scale factor (the curve 0.0a is the gapless case and 1.0a represents the standard case “a”). The PBF process ensues when the cooling curve for each gap separates from the upper (gapless) trajectory. The standard case 1.0a is seen to represent the most efficient neutrino emission and the most rapidly cooling case. All models are for  $1.4 M_\odot$  stars built using the EOS of APR (Akmal, Pandharipande & Ravenhall 1998) with heavy element compositions.

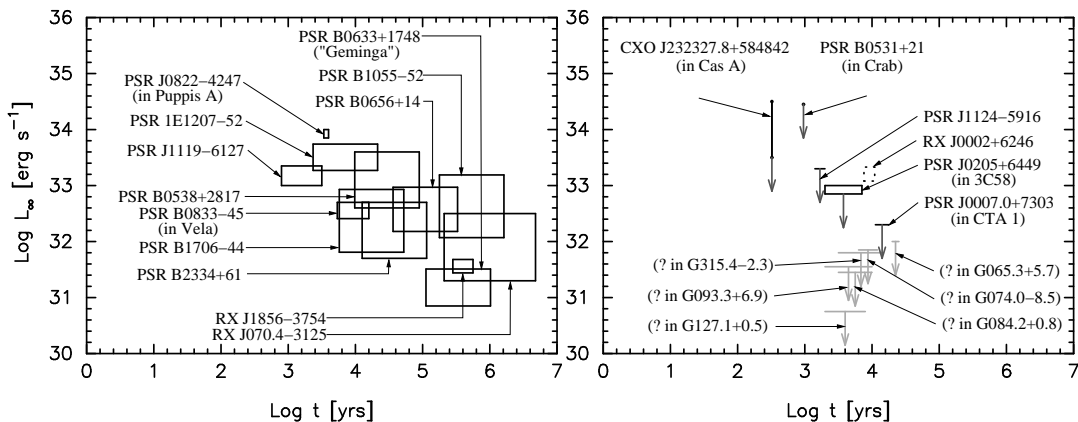


FIG. 8.— Summary of observational data on thermal luminosities of isolated cooling neutron stars. Left panel: 12 stars for which a thermal spectrum has been clearly detected. Right panel: the PSR in the nebula 3C58 seems to exhibit a thermal component, and could be presented in the upper panel, whereas in the case of the other objects a thermal component from the main stellar surface is not detected; consequently, the data shown are upper limits on the thermal luminosity. The labels “?” indicate that a compact object has not yet been detected in the supernova remnant. Finally, the object RX J0002+6246 in CTB1 is possibly not a neutron star (Esposito et al. 2008). See Appendix A for details.

would violate the compatibility conditions in equations (12) and (13) for minimal cooling. This density dependence, in particular an already large  $T_c$  at nuclear matter density, was inspired by the microscopic models of Baldo et al. (1998), and the compatibility conditions we find are a strong constraint against such types of gaps. However, in case the gap has a vanishingly small  $T_c$  at low densities, as the model “T”, and grows above  $0.5 \times 10^9$  K at higher densities, then it will inescapably cross the compatibility band, no matter how large is its  $T_c^{\text{max}}$ . It is intriguing that such strong constraints on the neutron triplet gap emerge for consistency of the minimal model with data.

#### 4. DISCUSSION AND COMPARISON WITH DATA

The observational data against which we will compare our results are displayed in Figure 8 and described in Appendix A. An extensive set of full neutron star cooling histories employing the minimal cooling scenario are displayed in Figure 9 from which the effects of the vector channel suppression of Cooper-pair emission can be discerned. A total of 300 cooling histories are shown and superposed with the data from Figure 8. Comparing the left and right column panels of Figure 9, it is clear that for times later than the crust thermal relaxation time ( $t \gtrsim 100$  years) the effects of suppressing Cooper pair emission from the vector channel are very small. Therefore, the major conclusions that were reached in Paper I concerning minimal cooling remain valid.

In order to highlight the scope and limitations of the minimal cooling paradigm, and to refine its implications, we recall its main conclusions as stated in Paper I. Given the uncertainties about the major physical ingredients, namely, the sizes of the various pairing gaps and the chemical composition of the envelope, the cooling curves of the minimal model appear to be consistent with data of nearly all neutron stars with observed thermal emission, as long as the coldest possible trajectories under the minimal cooling paradigm occur in some cases. The compatibility of nearly all neutron stars with minimal cooling requires strong conditions on the size of the neutron  ${}^3\text{P}_2$  gap and the chemical composition of the stellar envelopes, as discussed below.

A few exceptions exist, notably the pulsar in CTA 1, together with the unobserved emissions from several young



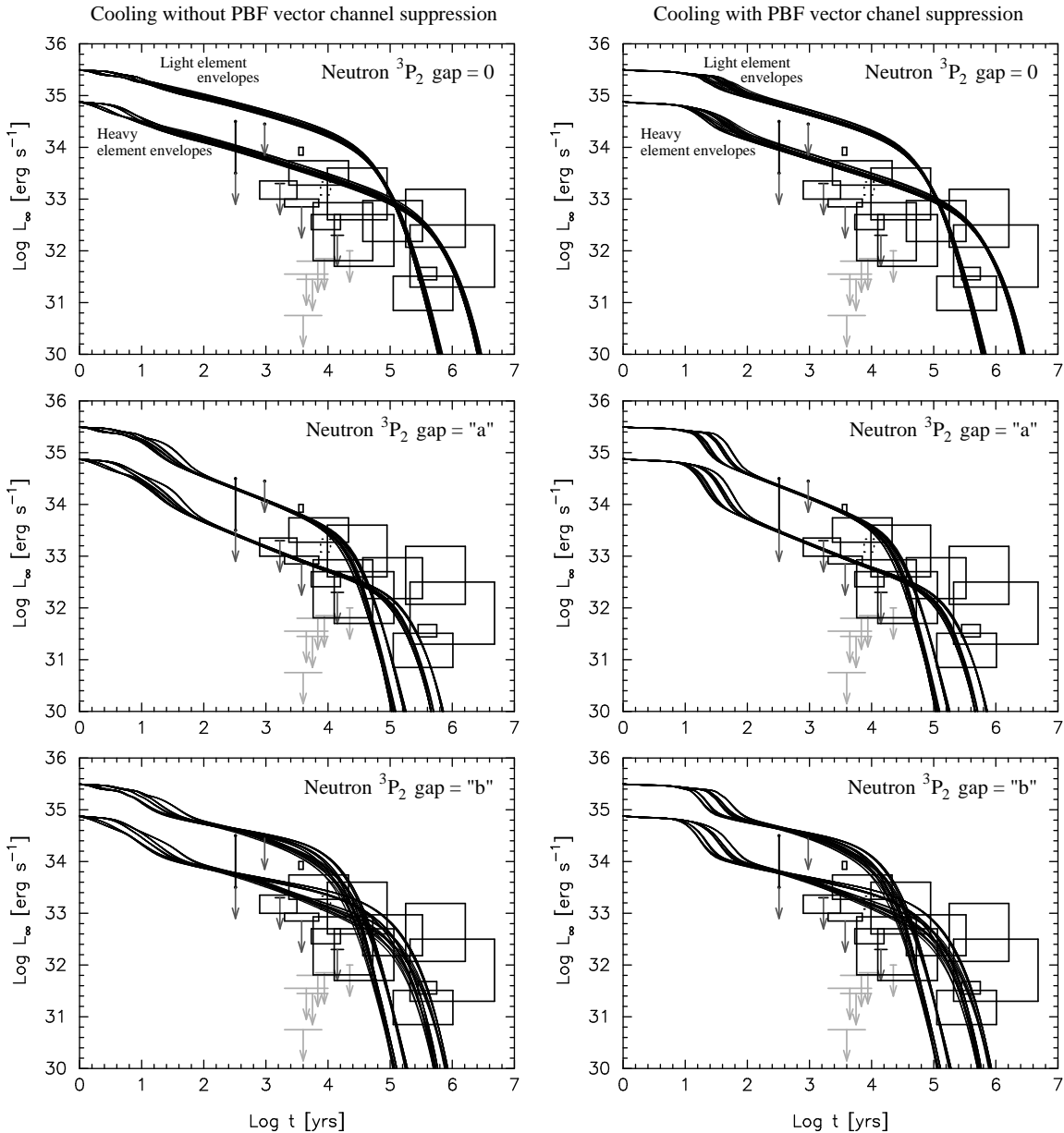


FIG. 9.— Comparison of predictions of the minimal cooling scenario with data; all models are for  $1.4 M_{\odot}$  stars built using the EOS of APR (Akmal, Pandharipande & Ravenhall 1998). In the right panels the suppression of the vector channel in the Cooper-pair neutrino emission is fully taken into account whereas, for comparison, in the left panels the suppression has been omitted. In each row, the two panels have the same neutron  ${}^3P_2$  gap, from a vanishing gap in the upper row to our model gaps “a” and “b” (following the notations of Figure 10 in Paper I) in the next two rows. In each panel two sets of cooling trajectories, either with light or with heavy element envelopes, are shown which include 25 curves corresponding to 5 choices of the neutron  ${}^1S_0$  and of the proton  ${}^1S_0$  gaps covering the range of predictions about the sizes of these gaps.

supernova remnants that might be reasonably expected to contain neutron stars, as they evidently lie below any of the minimal cooling histories displayed. These few objects, if confirmed, provide us with the most compelling evidence in favor of the occurrence of enhanced neutrino emission beyond the minimal cooling paradigm.

In the case that the  $T_c$  curve crosses the compatibility band as in our models “a” and “T”, agreement with data can be achieved if the warmest stars, such as the pulsar in Puppis A and PSR 1E1207-52, have light element envelopes, while the coldest ones, like PSR J1119-6127, the pulsars in 3C58 and Vela, and PSR J1124-5916, have heavy element envelopes. This agreement is lost, however, if the value of  $T_c^{\text{min}}$  is too large, i.e., greater than about  $0.2 \times 10^9$  K (see equation 13), as in our models “b” and “c”. In the extreme case that the neutron  ${}^3P_2$  gap is vanishingly small and also that all observed young cooling neutron stars have light element envelopes, then nearly all of them, with the possible exception of PSR B0538+2817, are observed to be too cold to be compatible with minimal cooling predictions. In the less extreme possibility of a heterogeneity in chemical composition and a vanishingly small neutron  ${}^3P_2$  gap, we still find that more than half (seven out of twelve) of the observed young cooling neutron stars are too cold to be

compatible with minimal cooling. (Notice that among the remaining five, out of twelve stars, the compact objects in Cas A and the Crab still have only upper limits.) If these conditions on the  $T_c$  curve are not satisfied for a particular model of superfluidity in dense matter, then that model also requires enhanced cooling beyond the minimal cooling paradigm. These results highlight the importance of the  $n$   ${}^3\text{P}_2$  gap in more precise terms than discussed in Paper I.

Our conclusion regarding the need for heterogeneity in the chemical composition of the atmosphere is consistent with the results of Kaminker, et al. (2006), who had to employ both light and heavy element atmospheres in their cooling models to match the data of most stars.

That it is apparently possible to explain the majority of thermally-emitting neutron stars with the minimal cooling paradigm led Klahn, et al. (2006) to propose the so-called direct Urca constraint which would effectively place limits on the density dependence of the nuclear symmetry energy. This follows from the fact that higher mass stars have larger central densities, so that the few stars that appear to be too cold could have larger than average neutron star masses. The nearly two dozen well-measured neutron star masses are mostly concentrated in the range 1.25–1.5  $M_\odot$  (Lattimer & Prakash 2005), although there are indications that some neutron stars might extend beyond the upper end of this range. Mass-dependent cooling in the context of direct Urca processes was suggested by Lattimer et al. (1991), and has been exploited by Page & Applegate (1992) and Yakovlev & Pethick (2004) to account for the gross features of cooling data. If rapid cooling is, in fact, due to the onset of the direct Urca process involving nucleons, as opposed to hyperons, kaon condensates, or deconfined quarks, a constraint on the density dependence of the nuclear symmetry energy could therefore result. The nuclear symmetry energy would have to grow relatively slowly with density so that the threshold density for the direct Urca process to occur exceeds the central density of most neutron stars, few of which could be very massive. The inferred constraints on the symmetry energy may also depend significantly on the presence of quartic terms in the symmetry energy (Steiner 2006).

However, if any of the assumptions in the above logical sequence are violated, the direct Urca constraint becomes invalid. Envelope compositions and the neutron  ${}^3\text{P}_2$  gap might be outside the required ranges. Perhaps even in massive neutron stars cooling due to the direct Urca process is abated due to superfluid-induced suppression. Furthermore, in the exceptional cases in which rapid cooling is suspected, it will be difficult to prove that the nucleon direct Urca is responsible as all proposed rapid cooling emission rates are orders of magnitude greater than modified Urca or Cooper-pair emission rates. It should also be noted that there are at present no reliable mass measurements of any thermally-detected cooling neutron stars, so that mass information deduced from binary pulsars might not be relevant.

## 5. SUMMARY AND CONCLUSIONS

Neutrinos emitted in the continual Cooper-pair breaking and formation (PBF) processes that occur near the critical temperatures of superfluid neutrons and superconducting protons in neutron star interiors are an integral part of the minimal cooling paradigm (Paper I). These processes were not generally included in the traditional standard cooling scenario, but are nevertheless expected to occur whether or not rapid cooling occurs. If all neutron star cooling data are found to be consistent with the predictions of the minimal cooling model, (in which rapid cooling by direct Urca processes occurring through reactions involving nucleons, hyperons, quarks, or Bose Condensates were eliminated by design) then there is no reason to invoke rapid cooling. Either rapid cooling does not occur or it is suppressed by superfluidity. In either case, constraints about the properties of dense matter ensue.

However, beginning with Leinson & Perez (2006a), several authors (Sedrakian, M  ther & Schuck 2007; Kolomeitsev & Voskresensky 2008; Leinson 2008; Steiner & Reddy 2008) have recently established that the PBF neutrino emissivity from the vector channel is suppressed by a factor of  $\sim 10^{-3}$  from the original estimates of Flowers, Ruderman & Sutherland (1976), who overlooked the conservation of vector current in weak interactions. In view of this development, we have performed extensive calculations to assess the effects of the severely reduced rates in the vector channel on the long-term cooling of neutron stars incorporating the revised PBF rates.

Our analysis leads us to conclude that the long-term cooling of neutron stars as envisaged in the minimal cooling paradigm is not significantly affected by the proposed large reductions in the vector channel of the PBF neutrino emissivities. The reason is that Cooper-pair emission occurs through both vector and axial channels, and the axial part of the Cooper-pair emission is barely affected. The axial channel of the PBF emissivities controls the long-term cooling, whereas the vector channel emissivities are important for the cooling behavior of neutron stars with ages less than a few hundreds of years for which observational data are not yet available. With the exception of few candidates (e.g., CTA 1 and perhaps unobserved stars in other remnants), the minimal cooling paradigm is consistent with observations of neutron star temperatures and ages, but, as noted in Paper I, only if certain combinations of light- or heavy-element envelopes and sizes of neutron triplet pairing gaps in the star’s core exist.

For the minimal cooling model to be consistent with data, it is necessary for the most efficient cooling possible to occur. Therefore, our analysis places a stringent requirement on the critical temperature for neutron superfluid pairing in the triplet channel in the core of the star. It is required that the  $T_c$  curve crosses the compatibility band described in Figure 4, and therefore the triplet gap must both become larger than  $T_c = 0.5 \times 10^9$  K at some moderately large density (but less than the central density of the neutron star), and also become smaller than  $T_c = 0.2 \times 10^9$  K (either at high density, i.e., in the center of the star, or at low density, i.e. in the outermost part of the core). If the gap does not fulfill these conditions, then observations point to the occurrence of enhanced cooling in at least half of the young isolated cooling neutron stars observed so far.

DGAPA grants of the PAPIIT program (#IN119306 and #IN122609). JML and MP acknowledge research support from the U.S. DOE grants DE-AC02-87ER40317 and DE-FG02-93ER-40756, respectively. JML would also like to acknowledge support from a Glidden Visiting Professorship Award at Ohio University. AWS is supported by the Joint Institute for Nuclear Astrophysics under NSF-PFC grant PHYS 08-22648, by NASA ATFP grant NNX08AG76G, and by the NSF under grant number PHY-0456903. The hospitality of the National Institute of Nuclear Theory, University of Washington, Seattle, USA, where this work was begun is acknowledged.

APPENDIX  
OBSERVATIONAL DATA

The observational data plotted in Figures 8 and 9 in the text deserve some comments. We have considered the same objects and data as reported in Paper I, but with modifications for the first five objects discussed below. We have also included some additional objects (see the last four objects below) for which data has become available since Paper I was published. Salient aspects of the modifications and new data are summarized here.

In many cases, the only way in which the ages of the objects can be estimated is by their spin-down ages  $2P/\dot{P}$ . However, there are many stars for which kinematic ages have also been obtained. Comparing kinematic and spin-down ages for the same objects often reveals discrepancies of factors of three or more in both directions. For example, SNR N157B has a determined age of less than 2000 years but a pulsar spin-down time of 5000 years, and PSR B1757-24 has an estimated age less than 39000 years and a spin-down age of 16000 years. For this reason, we have attached nominal error bars of a factor of three to those objects for which we only have spin-down information. To ignore this uncertainty could be misleading.

*PSR RX J0205+6449 in the nebula 3C58*

The supernova remnant 3C58 has been associated with the historical supernova SN 1181 (Stephenson & Green 1999) providing us with a pulsar age of 828 years. However, this proposed association has been challenged in recent years. Measurements of the remnant's expansion velocity compared to its size (at an assumed distance of 3.2 kpc) require an older origin. Optical observations of filament expansion (angular expansion) and filament line width (radial expansion) imply an age of 3000-4000 yrs and 2700-3500 yrs, respectively (Fesen et al. 2008), whereas radio measurements of the filament expansion would imply an age of 4500-7000 yrs (Bietenholz 2006). Moreover, modeling of the energetics of the pulsar wind nebula and its expansion need an age of 2000-3000 yrs (Chevalier 2004, 2005) or even 2000-5000 yrs from the recent X-ray observations of Gotthelf, Helfand, & Newburgh (2007). These ages are more in accord with the pulsar spin-down age of 5400 yrs. We will, henceforth, adopt a conservative age of 2000-7000 yrs, keeping in mind the possible SN 1181 association and the corresponding age of 828 yrs.

*PSR B0833-45 in the SNR Vela*

The kinematic age of the SNR we adopted in Paper I was taken from Aschenbach, Egger & Trümper (1995) who employed a distance of 500 pc (the PSR dispersion measure distance). Correcting this distance to 300 pcs (the VLBI parallax distance of Dodson et al. 2003) gives us an age of 5400-16000 yrs as emphasized by Tsuruta et al. (2009).

*RX J0007.0+7302 in the SNR CTA1*

We notice that the *Fermi* Gamma-Ray space telescope has detected pulsations at 315 ms from this compact source (Abdo et al. 2008) and measured its spin-down age as  $1.4 \times 10^4$  yrs, in agreement with the estimated age of the remnant,  $1.4 - 2.2 \times 10^4$  yrs.

*PSR 1055-52*

This pulsar's spin-down age is  $10^{5.73}$  yrs instead of  $10^{5.43}$  yrs which was erroneously adopted in Paper I.

*PSR 1E1207-52*

A lower limit on the spin-down age of this pulsar has been found to be 27 Myrs (Gotthelf & Halpern 2007) while the associated supernova remnant kinematic age is about 7000 yrs (within a factor 3). As in Paper I, we use the kinematic age from the SNR.

*PSR B2334+61 in the SNR G114.3+0.3*

Surface thermal emission has been detected in an XMM-Newton observation (McGowan et al. 2006). The distance estimate from the pulsar dispersion measure is  $3.1_{-1.0}^{+0.2}$  kpc, but HI absorption (Yar-Uyaniker et al. 2004) indicates a much shorter distance of less than 1 kpc. Fits of the spectrum with a magnetized hydrogen neutron star atmosphere (NSA) gives  $T_{\infty}^{NSA} = 0.65 \times 10^6$  K and  $R_{\infty}^{NSA} \sim 13$  km, whereas a blackbody (BB) fit gives  $T_{\infty}^{BB} = 1.6 \times 10^6$  K and  $R_{\infty}^{BB} \sim 1.6$  km. In both cases, a distance of 3.1 kpc was assumed. The hydrogen atmosphere model seems to give better fits, but the BB fit would be preferred in case of the smaller distance. However, the uncertainty on the luminosity is dominated by the uncertainty in the distance and with the above values, we obtain  $L_{\infty} = 0.5 \times 10^{32} - 5 \times 10^{32}$  erg  $s^{-1}$  using the NSA values, whereas the BB values give an  $L_{\infty}$  range included within the NSA results. The age of the SNR, a few times  $10^4$  yrs, is uncertain as is the association with the PSR whose spin-down age is  $4 \times 10^4$  yrs. We will adopt an age of  $(\frac{1}{3} - 3) \times t_{sd}$ , i.e., with the same uncertainty factor as we did in Paper I.

*PSR J1119-6127*

This high-field pulsar shows a thermal spectrum which when fitted by a blackbody spectrum gives  $L_{\infty}^{BB} = (1.35 - 2.25) \times 10^{33} \text{ erg s}^{-1}$ . NSA fits yield  $L_{\infty}^{NSA} = (1.05 - 2.05) \times 10^{33} \text{ erg s}^{-1}$  (Safi-Harb & Kumar 2008). The NSA fit is compatible with emission from the entire neutron star surface whereas the BB fit implies a much smaller radius ( $\sim 3.5$  km) at an estimated distance of 8.5 kpc. However, the distance is uncertain and the exceptionally high pulsed fraction ( $\sim 75\%$ ) (Gonzalez et al. 2005) may favor a small thermally emitting region. Given this and because  $L_{\infty}^{BB}$  and  $L_{\infty}^{NSA}$  are similar, we adopt  $L_{\infty}^{BB} = (1.05 - 2.25) \times 10^{33} \text{ erg s}^{-1}$  for the thermal luminosity. The spin-down age is  $t_{sd} = 1600$  yrs. As the measured braking index  $n = 2.9$  (Camilo et al. 2000) is compatible with magneto-dipolar breaking, and the characteristics of the associated SNR and the Pulsar Wind Nebula (PWN) are compatible with an age close to  $t_{sd}$  (Safi-Harb & Kumar 2008), we adopt an age estimate of  $(0.5 - 2) \times t_{sd}$ .

*PSR B0531+21 in the Crab nebula*

Phase resolved X-ray spectroscopy (Weisskopf et al. 2004) gives the most stringent upper limit on the surface thermal luminosity,  $L_{\infty} < 2.8 \times 10^{34} \text{ erg s}^{-1}$ . However, there is no evidence of a thermal component in the spectrum which is completely dominated by magnetospheric emission.

*SNRs G065.3+5.7 and G074.0-8.5*

In their extensive search for compact objects in nearby SNRs, Kaplan et al. (2006) provide six new upper limits on the thermal luminosity of possibly existing (but undetected) compact stars. Four of these limits are quite high so we will retain only the two lowest ones:  $L_{\infty} < 10^{32} \text{ erg s}^{-1}$  for SNR G065.3+5.7 (Cygnus Loop) and  $L_{\infty} < 0.7 \times 10^{32} \text{ erg s}^{-1}$  for G074.0-8.5. The estimated ages of the remnants are  $(2 - 2.5) \times 10^4$  yrs and  $(0.6 - 1.2) \times 10^4$  yrs, respectively.

## REFERENCES

- Abdo, A. A., et al. 2008, *Sci.* 322, 1218  
 Akmal, A. and Pandharipande, V. R., & Ravenhall, D. G. 1998, *Phys. Rev. C* 58, 1804  
 Amundsen, L., & Østgaard, E. 1985, *Nucl. Phys. A* 437, 487  
 Aschenbach, B., Egger, R., & Trümper, J. 1995, *Nature* 373, 587  
 Baldo, M., Elgarøy, Ø., Engvik, L., Hjorth-Jensen, M., & Schulze, H.-J. 1998, *Phys. Rev. C* 58, 1921  
 Bietenholz, M. F. 2006, *ApJ* 645, 1180  
 Bohr, A., Mottelson, B. R., & Pines, D. 1958, *Phys. Rev.* 110, 936  
 Brown, E. F., & Cumming, A. 2009, *ApJ* in press [e-print: arXiv:0901.3115]  
 Cackett, E. M., Wijnands, R., Linares, M., Miller, J. M., Homan, J., & Lewin, W. 2006, *MNRAS* 372, 479  
 Cackett, E. M., Wijnands, R., Miller, J. M., Brown, E. F., & Degenaar, N. 2008, *ApJ* 687, L87  
 Camilo, F., Kaspi, V. M., Lyne, A. G., Manchester, R. N., Bell, J. F., D'Amico, N., McKay, N. P. F., & Crawford, F. 2000, *ApJ* 541, 367  
 Chen, J. M. C., Clark, J. W., Davé, R. D., & Khodel, V. V. 1993, *Nucl. Phys. A* 555, 59  
 Chevalier, R. A. 2004, *Ad. Sp. Res.* 33, 456  
 Chevalier, R. A. 2005, *ApJ* 619, 839  
 Cumming, A., Macbeth, J., in't Zand, J. J. M., & Page, D. 2006, *ApJ* 646, 429  
 Degenaar, N., Wijnands, R., Wolff, M. T., Ray, P. S., Wood, K. S., Homan, J., Lewin, W. H. G., Jonker, P. G., Cackett, E. M., Miller, J. M., & Brown, E. F. 2009, *MNRAS* 221, in press. [e-print: arXiv:0811.4582]  
 Dodson, R., Legge, D., Reynolds, J. E., & McCulloch, P. M. 2003, *ApJ* 596, 1137  
 Esposito, P., de Luca, A., Tiengo, A., Paizis, A., Mereghetti, S., Caraveo, P. A. 2008, *MNRAS* 384, 225  
 Fesen, R., Rudie, G., Hurford, A., & Soto, A. 2008 *ApJS* 174, 379  
 Flowers, E., Ruderman, M., & Sutherland, P. 1976, *ApJ* 205, 541  
 Friman, B. L., & Maxwell, O. V. 1979, *ApJ* 232, 541  
 Gandolfi, S., Illarionov, A. Yu., Fantoni, S., Pederiva, F., & Schmidt, K. E. 2008, *Phys. Rev. Lett.* 101, 132501  
 Gezerlis, A. & Carlson, J. 2008, *Phys. Rev. C* 77, 032801(R)  
 Gonzalez, M. E., Kaspi, V. M., Camilo, F., Gaensler, B. M., & Pivovarov, M. J. 2005, *ApJ* 630, 489  
 Gotthelf, E. V., & Halpern, J. P. 2007, *ApJ* 664, L35  
 Gotthelf, E. V., Helfand, D. J., & Newburgh, L. 2007, *ApJ* 654, 267  
 Kaminker, A. D., Haensel, P., & Yakovlev, D. G. 1999, *A&A* 345, L14  
 Kaminker, A. D., Gusakov, M. E., Yakovlev, D. G., & Gnedin, O. Y. 2006, *MNRAS* 365, 1300  
 Kaplan, D. L., Gaensler, B. M., Kulkarni, S. R., Slane, P. O. 2006, *ApJS* 163, 344  
 Klähn, T., Blaschke, D., Typel, S., van Dalen, E.N.E., Faessler, A., Fuchs, C., Gaitanos, T., Grigorian, H., Ho, A., Kolomeitsev, E.E., Miller, M.C., Ropke, G., Trümper, J., Voskresensky, D.N., Weber, F., Wolteret H.H. 2006, *Phys. Rev. C* 74, 035802  
 Kolomeitsev, E. E. & Voskresensky, D. N. 2008, *Phys. Rev. C* 77, 065808.  
 Kundu, J., & Reddy, S. 2004, *Phys. Rev. C* 70, e5803K  
 Lattimer, J. M., Pethick, C. J., Prakash, M., & Haensel, P. 1991, *Phys. Rev. Lett.* 66, 2701  
 Lattimer, J. M., van Riper, K. A., Prakash, M., & Prakash, M. 1994, *ApJ* 425, 802  
 Lattimer, J. M., & Prakash, M. 2005, *PRL* 94, 1111011  
 Leinson, L. B. & Perez, A. 2006, *Phys. Lett. B* 638, 114  
 Leinson, L. B. & Perez, A. 2006, [e-print: arXiv:astro-ph/0606653].  
 Leinson, L. B. 2008, *Phys. Rev. C* 78, 015502.  
 McGowan, K. E., Zane, S., Cropper, M., Vestrand, W. T., & Ho, C. 2006, *ApJ* 639, 377  
 Page, D. 2009, in *Neutron Stars and Pulsars*, Ed. W. Becker, Springer Verlag, Astrophysics & Space Science Library, p. 247-288.  
 Page, D., & Applegate, J. H. 1992, *ApJ* 394, L17  
 Page, D., Lattimer, J. M., Prakash, M. & Steiner, A. W. 2004, *ApJ Supp.* 155, 623  
 Page, D., Geppert, U., & Weber, F. 2006, *Nucl. Phys. A* 777, 497  
 Pethick, C. J. 1992, *Rev. Mod. Phys.* 64, 1133  
 Prakash, M. 1994, *Phys. Rep.* 242, 297  
 Prakash, M. 1998, in *Nuclear and Particle Astrophysics*, ed. J. G. Hirsch, & D. Page (Cambridge: Cambridge University Press), 153  
 Prakash, M., Prakash, Manju., Lattimer, J. M., & Pethick, C. J. 1992, *ApJ* 390, L77  
 Rutledge, R. E., Bildsten, L., Brown, E. F., Pavlov, G. G., Zavlin, V. E., & Ushomirsky, G. 2002, *ApJ* 580, 413  
 Safi-Harb, S., & Kumar, H. S. 2008, *ApJ* 684, 532  
 Schwenk, A., Friman, B., & Brown, G. E. 2003, *Nucl. Phys. A* 713, 191  
 Schwenk, A., & Friman, B. 2004, *Phys. Rev. Lett.* 92, h2501  
 Sedrakian, A., Müther, H. & Schuck, P. 2007, *Phys. Rev. C* 76, 055805.  
 Shternin, P. S., Yakovlev, D. G., Haensel, P., & Potekhin, A. Y. 2007, *MNRAS* 382, L43

- Steiner, A. W. 2006, *Phys. Rev. C* 74, 045808
- Steiner, A. W. & Reddy, S. 2008, *Phys. Rev. C* 79, 015802
- Stephenson, F. R., & Green, D. A. 1999, *Astron. & Geophys.* 40, 27
- Takatsuka, T. 1972, *Prog. Theor. Phys.* 48, 1517
- Tsuruta, S. 1986, *Comments Astrophys.* 11, 151.
- Tsuruta, S., Sadino, J., Kobelski, A., Teter, M. A., Liebmann, A. C., Takatsuka, T., Nomoto, K., & Umeda, H. 2009, *ApJ* 691, 621
- Voskresensky, D. N., & Senatorov, A. V. 1987, *Sov. J. Nucl. Phys.* 45, 411
- Wambach, J., Ainsworth, T. L., & Pines, D. 1993, *Nucl. Phys.* A555, 128
- Weisskopf, M. C., O'Dell, S. L., Paerels, F., Elsner, R. F., Becker, W., Tennant, A. F., & Swartz, D. A. 2004, *ApJ* 601, 1050
- Yakovlev, D. G., Kaminker, A. D. & Levenfish, K. P. 1999, *A&A* 343, 650
- Yakovlev, D. G., & Levenfish, K. P. 1995, *A&A* 297, 717
- Yakovlev, D. G., & Pethick, C. J. 2004, *ARA&A* 42, 169
- Yar-Uyaniker, A., Uyaniker, B., & Kothes, R. 2004 *ApJ* 616, 247